Available online at www.sciencedirect.com

SciVerse ScienceDirect

Ceramics International 39 (2013) S595–S600

CERAMICS INTERNATIONAL

www.elsevier.com/locate/ceramint

Effect of crystallization in frits on the contact of Ag–Si under fast firing

Dongsun Kim, Seunggon Choi, Hyungsun Kim*

School of Materials Engineering, Inha University, 253 Younghyun-dong, Incheon 402-751 Korea

Available online 17 October 2012

Abstract

The thermophysical properties of glass in Ag pastes must be controlled to enhance the optimal cell performance. In order to verify the effect of crystallization of glass on the formation of Ag recrystallites on n^+ emitter, several glasses that crystallize with increase in the firing temperatures were fabricated. The glass transition temperature, crystallization peak temperature, and melting temperature were determined using a differential thermal analyzer. The crystallization phases of glasses were verified via X-ray diffraction. The microstructures between the Ag electrodes and Si emitter were characterized by using a scanning electron microscope. The experimental results indicate that crystallization of glass significantly influence the viscous flow with increasing temperatures, which in turn affects the interface structures between the Ag electrodes and Si emitter.

Keywords: B. Interfaces; C. Thermal properties; D. Glass

1. Introduction

Ag thick-films have been widely used for the upper side metallization of Si solar cells. These pastes primarily consist of Ag powder, glass frits, and vehicles for the desired rheological properties of the pastes [1]. Although only a tiny quantity of glass frits has been added to the Ag paste, these frits enable the connection of the metal film to the Si wafer during firing. In particular, frits induce the current paths between the Ag electrodes and Si emitter [2].

The contact formations between Ag and Si with PbO glass systems have been studied and reported [3]. The current path from Si to Ag electrode is formed by the direct interconnection between Ag electrode and Si emitter [4]. The tunneling between Ag recrystallites is partly formed in n^+ emitter and ultra-thin glass layer [5], and in a multi-step conduction through metal precipitations such as Ag and Pb in glass layers [6].

To control the interfaces between the Ag electrodes and Si is a key factor to improve the cell performances. Frits influence the thickness of glass layers, the distribution of recrystallites formed on n^+ emitter and the penetration depth of recrystallites into Si, which affects the series resistance (R_s) and shunt resistance (R_{sh}) [7,8]. It has been reported that crystallization of frits occurs at high temperature, which prevents the viscous flows of frits and the penetration of Ag into Si emitter, which in turn enables the improvement of the R_{sh} [9].

However, it is unclear whether crystallization occurs or not under fast firing conditions. In this study, glasses that crystallize with increase in the temperature were fabricated and the crystallization of frits under fast heating rate was investigated because in the real process the firing used to fabricate the Si solar cells completes within a few minutes [10]. In addition, the effects of glass crystallization on Ag-Si contacts during firing, in a belt furnace, were verified.

2. Experimental procedures

Multi-crystalline Si wafers of dimension 180 μm in thickness and $156 \times 156\ mm^2$ in size, were used as substrates, and solar cells were fabricated using a rapid thermal process (RTP). The cell fabrication process consists of acid etching process, which forms texture structures on both surfaces, and phosphorous diffusion of n-type Si using a $POCl_3$ source on the front surface. Then, it is followed by edge isolation using plasma etching in a microwave barrel reactor. After removing the phosphorus silicate glass in an HF solution, an amorphous silicon

*Corresponding author. Tel.: +82 32 860 7545; fax: +82 32 862 5546.
E-mail address: kimhs@inha.ac.kr (H. Kim).

0272-8842/$ - see front matter © 2012 Elsevier Ltd and Techna Group S.r.l. All rights reserved.
http://dx.doi.org/10.1016/j.ceramint.2012.10.143

Table 1
Compositions of glass frits used in this study (in mol%).

Glasses	PbO	SiO_2	Al_2O_3	ZnO	R_2O+RO_2 [R=Na, Li, Zr]	Sum
PS1	36.2	35.7	10.8	9.2	8.1	100
PS2	36.2	38.0	10.8	9.2	5.8	100
PS3	36.2	40.0	10.8	9.2	3.8	100

nitride antireflection layer SiN_x:H was deposited on the front textured surface using a common low frequency plasma-enhanced chemical vapor deposition system.

In order to prepare the glass frits, PbO–SiO_2–Al_2O_3–ZnO, R_2O and RO_2 (R–Na, Li and Zr: Aldrich, USA) oxide powders with more than 99 % purity (Table 1) were mixed in a ball mill for 12 h. The mixture was then melted in a Pt crucible at 1300 °C for 30 min and quenched on a ribbon roll. These glasses were crushed and milled under wet conditions using a planetary mono mill (Fritsch, Pulverisette-7, Germany). After wet milling, the distribution of frit sizes was analyzed using a particle size analyzer (LS230 & N4PLUS, Coulter Corporation, USA). The glass transition temperature (T_g), the onset temperature of crystallization (T_{oc}), crystallization peak temperature (T_{pc}) and peak melting temperature (T_{pm}) were determined using a differential thermal analyzer (TG-DTA, Rigaku, Japan) with a heating rate of 10 °C/min. The crystallization phases of frits were verified using a high resolution X-ray diffractometer (HR-XRD, X PET-PRO MRD, Japan).

Ag paste consisted of Ag (84 wt%), frits (4 wt%) and vehicles (12 wt%). The vehicles comprise ethylcellulose, α-terpineol ($C_{10}H_{18}O$), and 2-ethoxyethyl acetate ($C_6H_{12}O_3$). After depositing the pastes on the Si wafer, the Ag paste on the front and Al paste on the back of the wafer were co-fired via rapid thermal processing. The Ag bulk and glass layers were selectively removed using HNO_3 and HF solutions, and the interface structures between Ag electrodes and Si emitter after firing were characterized using a scanning electron microscope (SEM, Hitachi S-4300, Japan).

3. Results and discussion

3.1. Electrical properties of cells and thermal properties of frits

The electrical properties of the cells PS1, PS2 and PS3 with the Ag pastes after firing are shown in Table 2. Although the open-circuit voltage (V_{oc}) and short-circuit current (J_{sc}) of all the cells were the same, the fill factor (FF) of each cell with frits (PS1, PS2, PS3) increased to 76.3 and then decreased to 73.03% (in Table 2). This phenomenon indicates that the FF was influenced by the thickness of glass layers between the Ag electrodes and Si, and by the penetration of the Ag into the pn junction,

Table 2
IV-parameters of each cell with Ag pastes to which different frits were added.

Glasses	J_{sc} [mA/cm^2]	V_{oc} [V]	FF [%]	Efficiency [%]
PS1	33.97	0.61	74.9	15.6
PS2	34.00	0.61	76.3	15.9
PS3	34.04	0.61	73.0	15.3

Table 3
DTA results and powder size distribution of each frit.

Glasses	[a]T_g [°C]	[b]T_{oc} [°C]	[c]T_{pc} [°C]	[d]T_{pm} [°C]	$T_{oc}-T_g$ [°C]
PS1	447	710	719	769	263
PS2	459	691	705	767	232
PS3	476	622	769	x	146

x: The melting did not occur up to 800 °C.
[a]T_g is the glass transition temperature;
[b]T_{oc} is the onset temperature of crystallization;
[c]T_{pc} is the crystallization peak temperature;
[d]T_{pm} is the peak melting temperature.

which affects the series resistance (R_s) and the shunt resistance (R_{sh}) [7,8].

The range of T_g for the glass frits was controlled from 447 to 476 °C by changing the ratio of $SiO_2/(R_2O+RO_2)$ (in Table 3). The crystallization of glasses occurred at 710, 691 and 622 °C respectively with different compositions (PS1, PS2 and PS3). The glass range, as a glass forming stability, expressed by the temperatures difference observed during heating $\Delta T=T_{oc}-T_g$, is an indicator for the degree of reaction between Ag and Si.

When the value of this difference is high (PS1), the crystallization process is delayed. Although the peak melting temperature of crystallites in the glasses occurred at 769 and 767 °C for PS1 and PS2, respectively, the melting temperature of crystallites was not measured for PS3, in the range of 700 and 800 °C. The results suggest that the crystallites occurred in the glass (PS3) with increasing temperatures and did not melt up to 800 °C.

In addition, the particle sizes of each frit were similarly controlled in order to prevent size effects on the crystallization of the glass during firing. The mean sizes of the powders (PS1, PS2 and PS3) were 1.7, 1.9 and 2 μm, respectively.

3.2. Crystallite phase of frits under different heating rates and microstructures between Ag and Si after firing

The phase of crystallites occurred in the glasses was identified as $PbZnSiO_4$, which corresponds to JCPDS No. 74-1127 (Fig. 1). As the heating rate increased from 10 to 600 °C/min, the crystallinity of frits (PS1, PS2) decreased and the crystallization in the glasses (PS1 and PS2) at 600 °C/min did not occur. These phenomena indicate that crystallization does not arise from the fast heating rates,

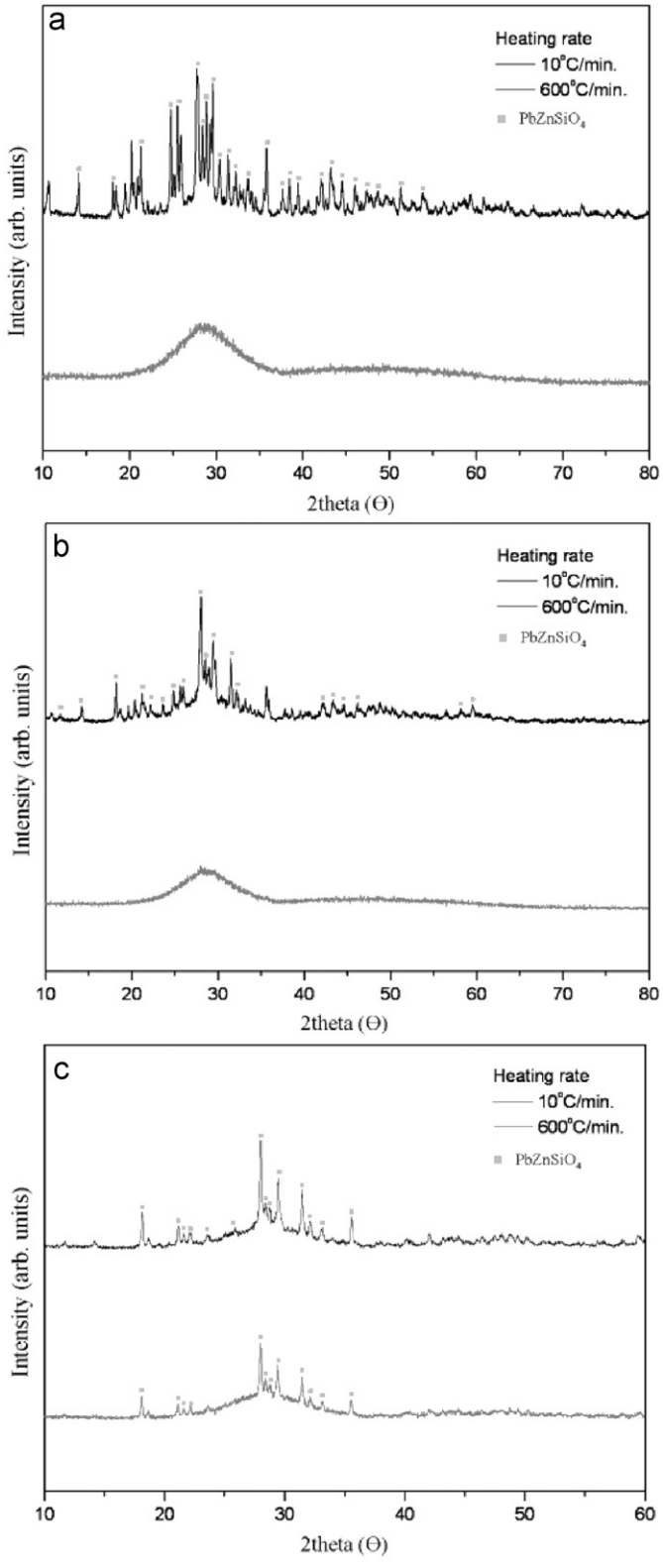

Fig. 1. XRD results of (a) PS1, (b) PS2 and (c) PS3 frits fired with different heating rates. The heating was performed at a rate of 10 and 600 °C/min. With the increase of the heating rates, the crystallization of the glasses was hindered. The peak firing temperature of glasses was 800 °C.

which delays the nucleus formation and crystal growth. Furthermore, although the crystallization of $PbZnSiO_4$ occurred in glasses (PS1 and PS2) during firing, the crystallites would melt around the peak melting temperatures (769 and 767 °C) as seen in Table 3.

Although the frits (PS3) were fired under a heating rate of 600 °C/min., the crystallization of the $PbZnSiO_4$ in the glass occurred due to the melting temperature being above 800 °C. These results are in agreement with the experimental studies in the lead glass system ($PbO–ZnO–B_2O_3–SiO_2$) that Zhang et al. studied [11]. It is considered that

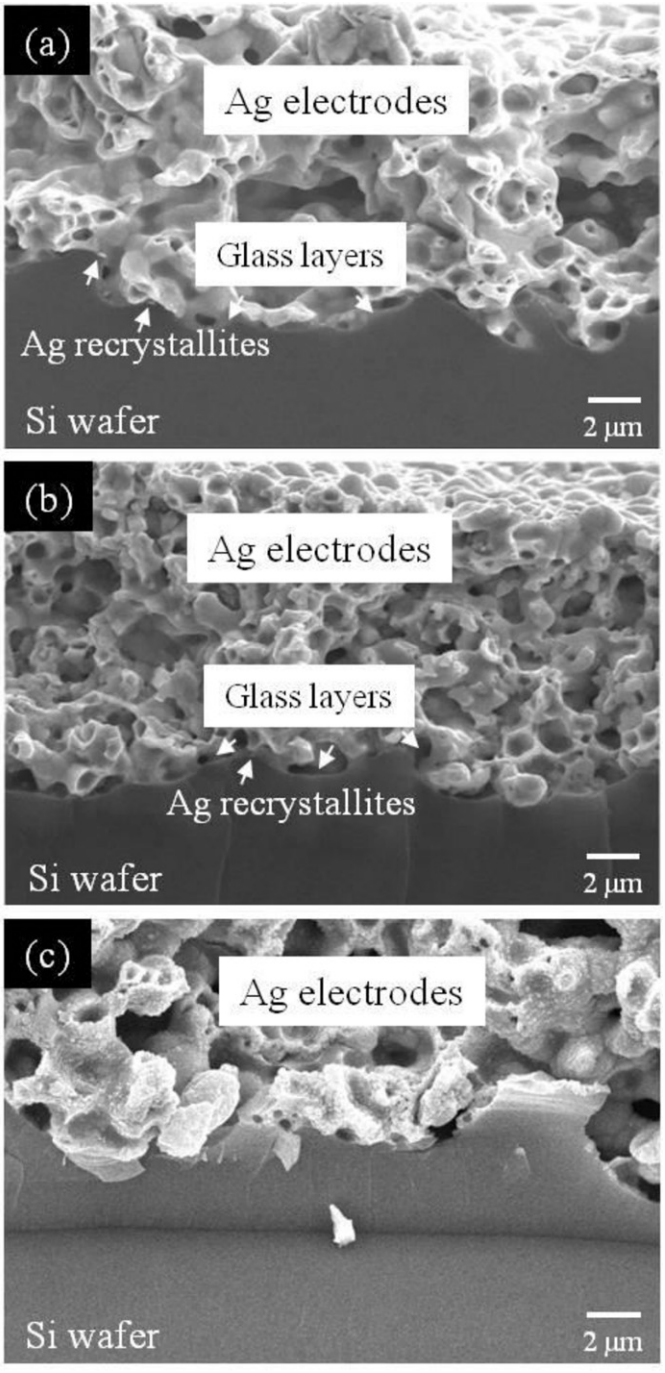

Fig. 2. Cross-sectional SEM images between Ag electrodes and Si wafer with (a) PS1, (b) PS2 and (c) PS3 in Ag pastes after firing. The firing was conducted in a belt furnace within 1 min. at a peak temperature of 800 °C.

the crystallization of $PbZnSiO_4$ in the glass under fast firing would occur as follows:

$$PbO\ (in\ glass) + ZnO\ (in\ glass) + SiO_2(in\ glass) \rightarrow PbZnSiO_4(crystallites) \quad (1)$$

Fig. 2 shows the cross-sectional SEM images between the Ag electrodes and Si with the different frits (PS1, PS2 and PS3) in the Ag pastes after firing. The interface structures of the Ag electrodes/glass layers/recrystallites penetrated into the Si wafer were formed with PS1 and PS2 (Fig. 2).

The glass layers and recrystallites between the Ag electrodes and Si were measured with PS1 and PS2 (Fig. 2(a) and (b), respectively), but were difficult to detect with PS3 (Fig. 2(c)). The recrystallites were formed on the Si wafer as shown Fig. 3 after the Ag electrodes and glass layers were removed. The number of recrystallites formed on the n^+ emitter decreased from 426 to 84 with the different frits (PS1, PS2 and PS3) in the area of 114 μm^2.

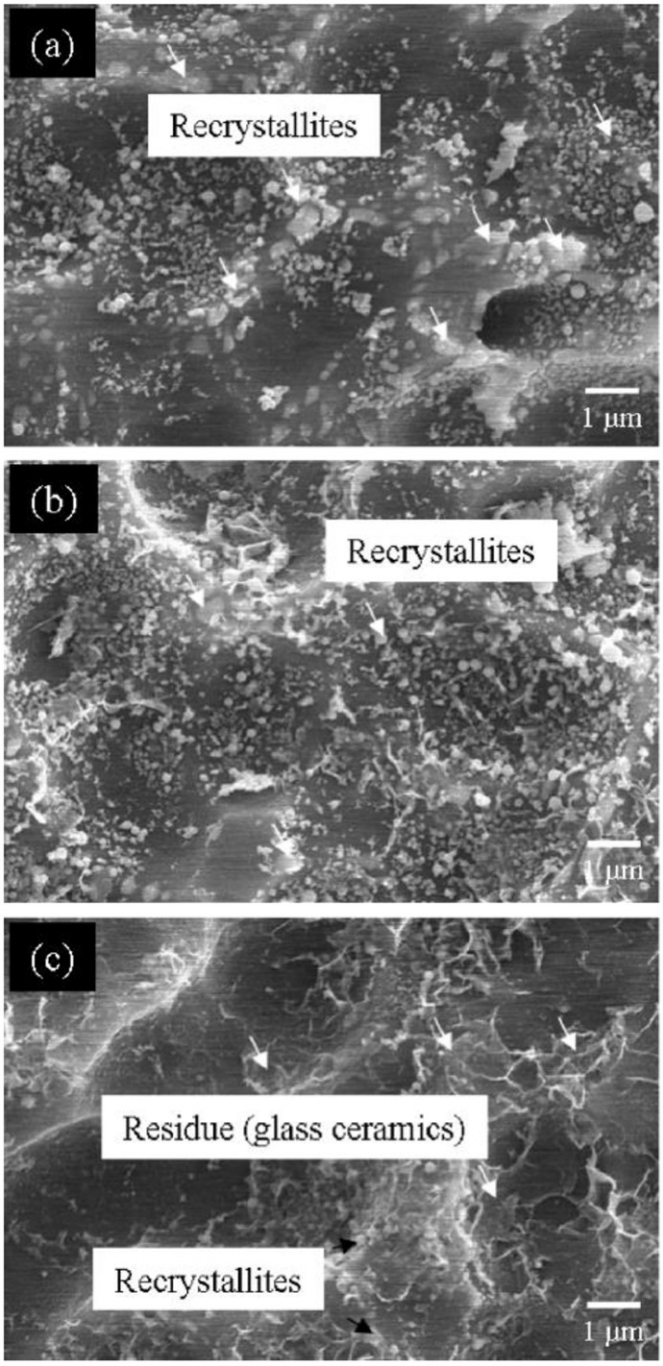

Fig. 3. Surface SEM images of recrystallites formed on the n^+ emitter with (a) PS1, (b) PS2 and (c) PS3 after removing Ag electrodes and glass layers. The residue (in Fig. 3c) indicates the glass ceramics.

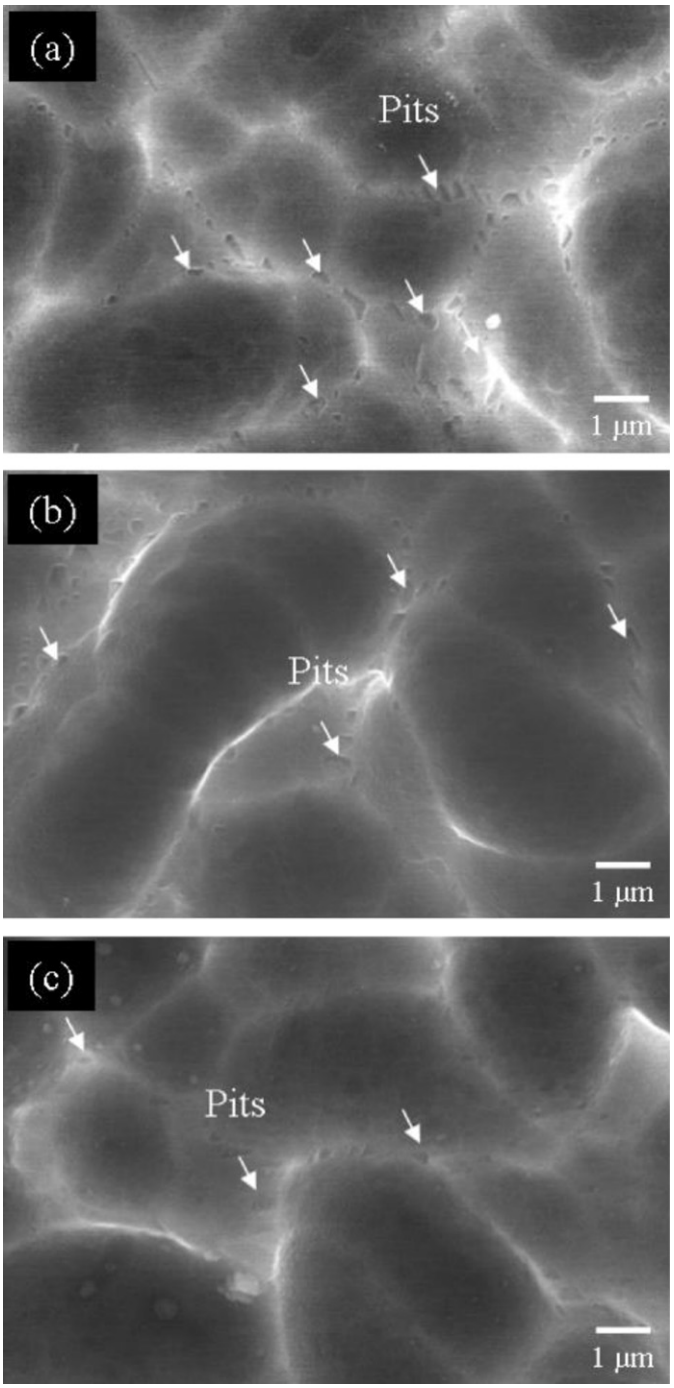

Fig. 4. Surface SEM images of pits formed into Si wafer with (a) PS1, (b) PS2 and (c) PS3 after removing recrystallites.

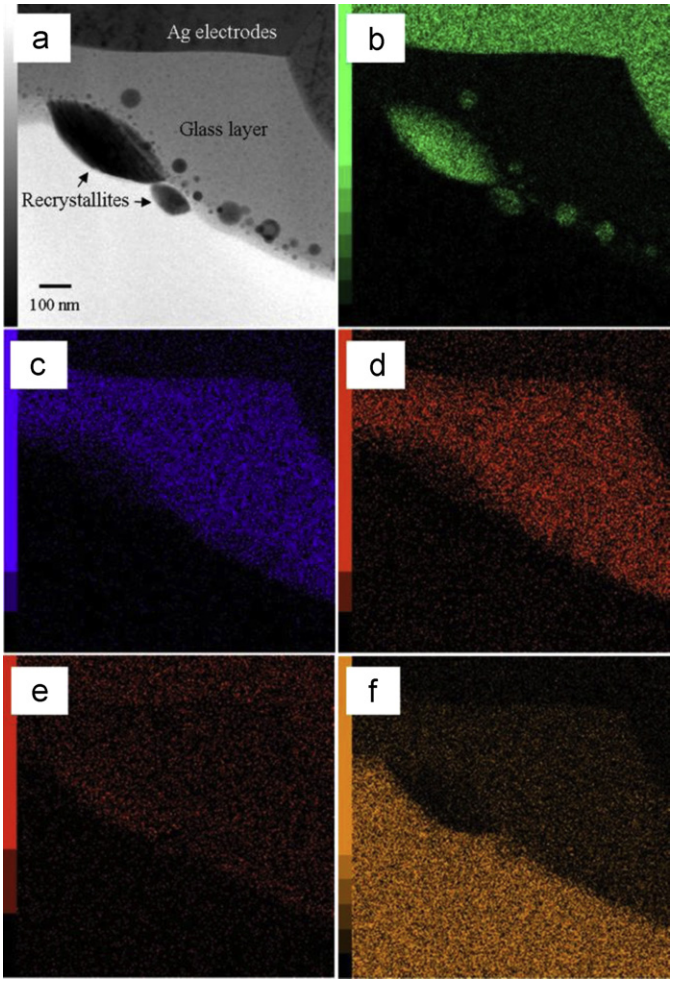

Fig. 5. (a) Cross-sectional STEM Z-contrast image and corresponding EDX compositional maps for (b) Ag, (c) Pb (d) O, (e) N and (f) Si atoms taken from the Ag contact on textured Si solar cells with PS1.

The maximum recrystallite size was also reduced from 0.62 to 0.04 μm^2 (Fig. 3(a)–(c)).

Many pits remained in the Si wafer after removing recrystallites penetrated into Si (Fig. 4). The size and number of the pits in the Si decreased in order of the PS1, PS2 and PS3 frits.

The reactions between the Ag, frits and Si would be hindered with the crystallization in glass during firing, which is resulted from a small ΔT (Table 3). The recrystallites penetrated into Si were verified as Ag using the STEM results with the PS1 in the Ag pastes after firing as shown in Fig. 5. EDX mapping clearly resolved the elemental distribution in the sample. The numerous Ag recrystallites were embedded in the glass layers and penetrated into the Si emitter. Furthermore, it is considered that the detection of N (as in Fig. 4(e)) would be attributed the redox reaction [12]:

$$2PbO\ (in\ \ glass) + SiN_{x(s)} \rightarrow 2Pb_{(l)} + SiO_2(in\ \ glass) + x/2N_{2(g)} \quad (2)$$

These results agree well with the previous results in which the PbO glasses were added to Ag pastes [5,13].

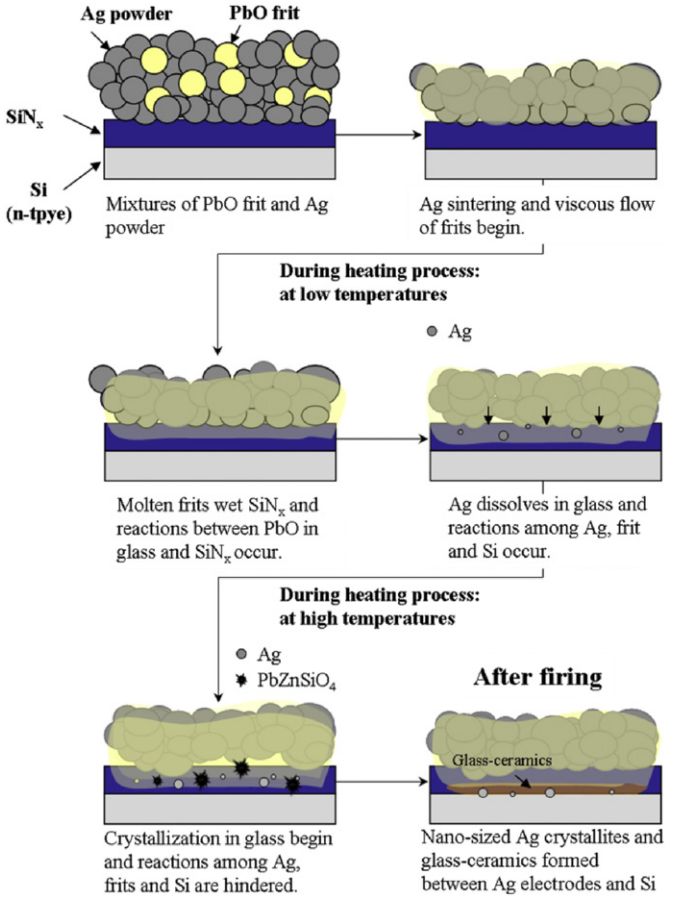

Fig. 6. Schematic diagram of Ag–Si contacts with the formation of crystallization in glass during firing.

The formation of Ag recrystallites would be influenced by the crystallization in the glass during firing. These phenomena can be explained using the schematic diagram in Fig. 6. The sintering of Ag powders began during the firing at low temperatures and the frits wet the surface of SiN_x layers with their viscous flows. A redox reaction between the PbO in the molten glass and SiN_x occur and Ag dissolved in the glass at high temperatures and penetrated the Si emitter [3]. However, the crystallization in the glass in the high temperature region hindered the dissolution of the Ag in glass with the high viscosity of frits, which resulted from the $PbZnSiO_4$ crystallites in the glass matrix during firing (Fig. 6). Therefore, the crystallization in glass during firing can affect the formation and penetration of Ag on and into Si emitters. A higher crystallinity in the glass would have an adverse effect on the electrical properties of the cells (Table 2).

In summary, it is expected that the current paths of electrons from n^+ emitter to Ag electrons would be through the thin glass/partly formed Ag recrystallites penetrated into n^+ emitter and the tunneling via metal precipitates such as Ag as shown in Fig. 7 [5,6].

However, it is believed that the glass ceramics formed in glass layers during firing can hinder the flow of electrons to

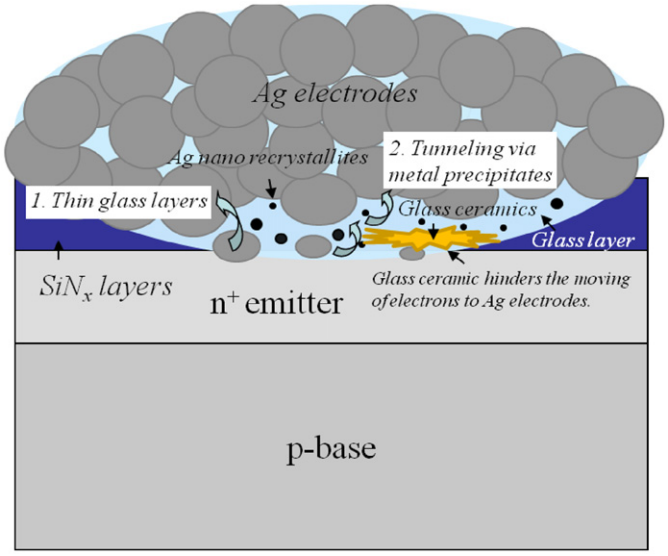

Fig. 7. Schematic diagram of Ag–Si contacts with the formation of crystallization in glass during firing.

Ag electrodes thus degrades FF, which is attributed to the series resistance (R_s).

4. Conclusion

The effects of crystallization in the glass (PbO–ZnO–Al_2O_3–SiO_2) during firing on the contacts of Ag–Si were studied. The nano-sized Ag recrystallites and the small sized pits were developed on the Si emitter with the crystallization in glass. The glass-ceramic ($PbZnSiO_4$) between the Ag electrodes and Si wafer were produced, which is attributed to the crystallization in the glass during firing. The crystallization of glass prevents the viscous flows of frits and the penetration of Ag into the Si emitter. We propose that the crystallization in glass interrupts the move of electrons from Si to Ag electrodes and degrades the cell performances.

Acknowledgments

This work is the outcome of a Manpower Development Program (2009-N-BL-HM-2-03-0000) for Energy & Resources supported by the Ministry of Knowledge and Economy (MKE) and is supported by the Pioneer Research Center of the National Research Foundation of Korea, funded by the Ministry of Education, Science and Technology (2011-0001685).

References

[1] S.B. Rane, T. Seth, G.J. Phatak, D.P. Amalnerkar, Effect of inorganic binders on the properties of silver thick films, Journal of Electronic Materials 15 (2004) 103–106.
[2] M. Prudenziati, L. Moro, B. Morten, F. Sirotti, L. Sardi, Ag-based thick-film front metallization of silicon solar cells, Active and Passive Electronic Components 13 (1989) 133–150.
[3] G. Schubert, F. Huster, P. Fath, Physical understanding of printed thick-film front contacts of crystalline Si solar cells—review of existing models and recent developments, Solar Energy Materials and Solar Cells 90 (2006) 3399–3406.
[4] G.C. Cheek, R.P. Mertens, R. Van Overstraeten, L. Frisson, Thick-film metallization for solar cell applications, IEEE Transactions on Electron Devices 31 (1984) 602–609.
[5] C. Ballif, D.M. Huljić, G. Willeke, A. Hessler-Wysser, Silver thick-film contacts on highly doped n-type silicon emitters: structural and electronic properties of the interface, Applied Physics Letters 82 (2003) 1878–1880.
[6] G. Schubert, B. Fischer, P. Fath, Formation and nature of Ag thick film front contacts on crystalline silicon solar cells. In: Proceeding of the Photovoltaics in Europe Conference, Rome, 2002, pp. 343–346.
[7] M.M. Hilali, M.M. Al-Hassim, B. To, H. Moutinho, A. Rohatgi, S. Asher, Understanding the formation and temperature dependence of thick-film Ag contacts on high sheet-resistance Si emitters for solar cells, Journal of the Electrochemical Society 152 (2005) G742–G749.
[8] D.S. Kim, S.J. Hwang, H.S. Kim, Effect of the thermal properties of frits on the electrical properties of screen-printed silicon solar cells, Journal of the Korean Physical Society 55 (2009) 1046–1050.
[9] M.M. Hilali, S. Sridharan, C. Khadilkar, A. Shaikh, A. Rohatgi, S. Kim, Effect of glass frit chemistry on the physical and electrical properties of thick-film Ag contacts for silicon solar cells, Journal of Electronic Materials 35 (2006) 2041–2047.
[10] D.H. Neuhaus, A. Munzer, Industrial silicon wafer solar cells, Advances in Opto Electronics 2007 (2007) 1–15.
[11] Y. Zhang, Y. Yang, J. Zheng, G. Chen, C. Cheng, C.M. Hwang, B.S. Ooi, A. Kovalskiy, H. Jain, Effect of the interface glass on electrical performance of screen printed Ag thick-film contacts of Si solar cells, Thin Solid Films 518 (2010) e111–e113.
[12] K.K. Hong, S.B. Cho, J.S. You, J.W. Jeong, S.M. Bea, J.Y. Huh, Mechanism for the formation of Ag crystallites in the Ag thick-film contacts of crystalline Si solar cells, Solar Energy Materials and Solar Cells 93 (2009) 898–904.
[13] M.I. Jeong, S.E. Park, D.H. Kim, J.S. Lee, Y.C. Park, K.S. Ahn, C.J. Choi, Transmission electron microscope study of screen-printed Ag contacts on crystalline Si solar cells, Journal of the Electrochemical Society 157 (2010) H934–H936.